A Self-adaptive Local Feature Extraction Based Magnetic Resonance Imaging

Jun Zhang[1], Tiantian Xu[1], Yuanjing Feng[1], Ye Wu[1], Yongqiang Li[1], Jianzhong He[1], Siqi Zhou[1]

1. Institute of Information Processing and Automation, Zhejiang University of Technology, Hangzhou, 310023

E-mail: fyjing@zjut.edu.cn

Abstract: Diffusion-weighted imaging and tractography can get information related to the macroscopic structure in vivo. High angular resolution diffusion imaging (HARDI), which offers a wide range of sampling data, has proven to better characterize complex intra-voxel structures compared to its predecessor diffusion tensor imaging (DTI). On the basis of HARDI, the data-driven approaches, such as spherical deconvolution (SD), become the emphasis of research in the field of brain. In this work, we substitute the spherical harmonics by a dictionary basis in SD, and incorporate a fiber orientation distribution function (fODF) based on SD, into a local feature extraction, which allows to form an self-adaptively sparse dictionary basis. The required fODF can be estimated from diffusion data and could be recalibrated with the data. In addition, the total variation of fODF is produced as auxiliary means. Verification is implemented on phantom and real data, which demonstrate that this data-driven approach can improve tomography result.

Key Words: Data-driven, Tractography, Dictionary Basis, Local Feature Extraction

1 INTRODUCTION

Magnetic resonance imaging (MRI) provides a unique, non-invasive technique to study the macroscopic structure and connectivity of brain white matter in vivo. Diffusion weighted MRI (DW-MRI) is currently the only method capable of mapping the fiber architecture of tissue in vivo and, as such, it has triggered tremendous hopes and expectations [1]. Diffusion Tensor Imaging (DTI) provides a powerful tool for mapping neural histoarchitecture. However, DTI has been shown to be inadequate in voxels containing multiple fibre orientations due to the constraints of the tensor model [2]. The appearance of high angular resolution diffusion imaging (HARDI) signal bring the hope to imaging of multiple fiber. The researchers pay attention to the large diffusion datasets, which can be used by data-driven approaches to derive the fiber geometry with as few prior assumptions about its physical properties as possible [3]. The most representational among these are q-ball imaging (QBI) techniques, which reconstruct the fiber orientation distribution function (fODF) based on a completely model-free reconstruction scheme named spherical tomographic inversion [4]. However, although QBI provides a much-improved description of the diffusion, it does not provide the actual fiber orientations [5]. At present, the more effective data-driven method called constrained spherical deconvolution (CSD) which reconstruct the fODF based on a fiber response function that may be estimated from the diffusion data itself is put forward by Tournier [2]. The higher order of the spherical harmonic base the better angular resolution between crossing fibers. However, spherical deconvolution model involves highly ill-conditioned solutions when used to solve the deconvolution problem [6]. It also requires estimating $(order+1)(order+2)/2$ unknown coefficients related to the spherical harmonic order; such requirement may lead to numerical instabilities and physically meaningless results (e.g., negatives or complex coefficients do not correspond to any physical meaning) [7]. In the regularization of solutions, even small changes in the noise levels of DW-MRI signals can lead to non-physical results [8]. Recently, methods accurately reconstructing the fODF with sparse dictionary attract many researchers' attention. [9] proposes a mathematical framework to register multi fascicle models (MFM), which defines novel operators to achieve interpolation, smoothing and averaging of multi-fascicle models. In fact, diffusion MRI at the imaging resolution available nowadays is sensitive only to the major fiber bundles and it is commonly accepted that it can reliably disentangle up to 2-3 different fiber populations inside a voxel [10]. We would like to choose the minimal number of fascicles that best represent the data observed. Specifically, [11] obtain this sparse solution and control for over-fitting using Elastic Net [12]. However, only exploiting the sparsity within a neighbourhood for the current patch is not optimal for the denoising task [13].

Because of the limitations of aforementioned approaches, a new method which is more precise and stable is required. A key point of our work is to implement a similar sparsity decomposition approach in the context of sparse coding model to nonlocal by grouping similar patches and forcing them to use the same dictionary atoms with different sparse codes. In this paper, we introduce a data-driven method that can self-adaptively construct dictionary bases from diffusion data with a local feature extraction process. We have

This work is supported by National Natural Science Foundation of China (NO.61379020), and Natural Science Foundation of Zhejiang Province (NO.LY13F030007).

been recognized early on that diffusion is consistent to the surrounding fiber geometry, and the specific link between both is essential for accurate and robust interpretation of sparse dictionary.

2 METHODS

2.1 Spherical Deconvolution Model with Data-driven

A lot of approaches aim to estimate an orientation distribution function (ODF) from the diffusion data. The ODF is a spherical distribution function which represents, as a probability distribution, the probability of something having a particular given orientation and is effectively a 3 dimensional, spherical realisation of a probability distribution function (PDF) [14]. Among these techniques, those who estimate the fODF which represents the probability that a fiber exits in the voxel with a particular given orientation, give a new way to exploit the fiber intra-voxel architecture.The most representative approach must be the spherical deconvolution, whose expression is as follows:

$$s\left(\boldsymbol{g}|\,\boldsymbol{u}\right)=\int_{\mathbb{S}^2} r\left(\boldsymbol{g},\boldsymbol{v}\right) f\left(\boldsymbol{v}|\,\boldsymbol{u}\right) d\mu\left(\boldsymbol{v}\right)+\xi \qquad (1)$$

where ξ is the noise,which is the main factors affecting the quality of the imaging. As a most widely used data-driven technique, spherical deconvolution [5] method directly describes fiber anatomy as the convolution of a kernel $r(\boldsymbol{g},\boldsymbol{v})$ with a fODF $f(\boldsymbol{v}\,|\boldsymbol{u})$. However, the spherical deconvolution only take the current voxel's structure and noise into consideration,ignoring the correlation between neighbouring voxels. Hence, a new model of data-driven spherical deconvolution have been proposed and can be simplified:

$$f^c=f\left(c,\Omega_c,\xi\right) \qquad (2)$$

where Ω_c is the neighbourhood information of fODF, which can drive the current voxel's fiber to find its appropriate direction, c is the current voxel's structure.

2.2 Regularization of the Local fODFs

In intravoxel fODF field, voxels within a small neighbourhood usually consist of similar structure. Thus, the fODFs derived from voxels' informations are ought to have a correlation in spatial structure. However, similar patches sometimes admit very different estimates due to the potential instability of sparse decompositions, which can result in noticeable reconstruction difference. Voxel-by-voxel methods for fiber configuration reconstruction commonly fail to ensure the spatial correlation as it just estimate the current voxel's fODF. Recent studies show that the spatial correlation between neighbouring voxels can be indirectly incorporated through a joint sparsity model [15] by assuming that the underlying sparse vectors associated with these pixels share a common sparsity support. Therein, a regularization of fODF data is used to make a preprocessing work. Consider voxels in a small neighbourhood of T (such as $3\times3\times3$) voxels. Let $\tilde{F}=\left[\tilde{f}_1,\tilde{f}_2,...,\tilde{f}_T\right]\in R^{n\times T}$ represent a matrix whose columns correspond to intravoxel fODF in a spatial neighbourhood in a magnetic resonance image. This matrix can be represented as a linear invariant with respect to a new joint sparsity matrix $F=[f_1,f_2,...,f_T]$, sharing the same support. The row-sparse matrix F can be recovered by solving the following proximal operators on matrices.

$$\underset{F}{min}\frac{1}{2}\left\|\tilde{F}-F\right\|_F^2+\lambda_1\|F\|_{1,2}+\lambda_2\sum_j\|F_j\|_1 \qquad (3)$$

where F_j is the j-th column of F. The former leads to a convex norm, while the latter actually counts the number of non-zero row and is only a pseudo norm. Hence, by forcing similar patches to admit similar decompositions, we successfully ensure the similarly spatial structure in fODF field.

2.3 Data-driven Local Feature Extraction for Dimensionality Reduction Imaging

Generally, fODF can be represented by an over-complete dictionary as mentioned in [16]. However, the dictionary is always redundancy. It could actually be represented by a quite sparse dictionary due to the spatial continuity among the neighbourhood voxels. The fact that the dictionary basis would be sharply peaked along the fODF is inherently appropriate. As the fODF represents the estimated distribution of fiber orientation inside each voxel directly, it encapsulates the information for tractography much more comprehensively. In a single voxel, the sparse dictionary would be acquired along the current voxel's fiber direction. The process can be expressed as: $f_i^c\rightarrow\left\{\wp_{v_j^i}^c|v_j^i,\ j=1,...,n_i\right\}$, where $\wp_{v_j^i}^c$ is the dictionary basis extracted from the current voxel fiber direction, v_j^i represents the fiber orientations obtained from the current voxel's fODF, n_i is the number of dictionary basis. Considering the anatomical fiber tracts through the brain have a natural quality of smoothness, there is a certain spatial coherence of fODFs in the neighbouring voxels, indicating that the fiber orientations are sparse and tend to be centralized. Therefore, we can infer that the dictionary used to represent the fiber orientation could be acquired from the local orientation distribution features extracted from neighbouring voxels' fODF. The final dictionary can be simplified as: $F\rightarrow\left\{\wp_{v_j^i}^c|v_j^i,\ \ j=1,\ldots,n_i,\ \ i=1,\ldots,\mathrm{T}\right\}$, which greatly decreases the dimensionality of dictionary basis and promote computational efficiency.

The joint sparsity model helps to regulate fODF structures and improve the sparsity of reconstructed fiber configuration. And the local features could be easily obtained by searching peaks of fODFs derived from diffusion data of voxels nearby. Thus, the center fODF could be represented by the sparse, new orientation distribution basis. Let $\sum_{v_j}\wp_{v_j}^c$ map to a new dictionary field. Then, we can rebuild a linear weighted combination to express the unknown fODF using these dictionary:

$$f\left(c,\Omega_c,\xi\right)=\sum_j\sum_{v_j^i}w_{v_j^i}\wp_{v_j^i}^c+\xi \qquad (4)$$

where $\omega_{v_j^i}$ is the unknown coefficient. Note that all the new dictionary bases are acquired from neighbour voxels' information, in the region of interest, fiber configuration of each voxel could be self-adaptively reconstructed with the features extracted from signals around.

In addition, considering that the neighbouring voxels have a similarity with the center intra-voxel architecture because of the spatial structure continuity, each voxel has an influence on the center one's construction more or less. The weights of effects from neighbour voxels are different but could be measured by the similarity between each other, which we will introduce in the next section.

2.4 Cost Function of new Spherical Deconvolution based Model with Total Variation

The regularization of fODFs and local features extracted from measure data make it possible to construct a relative sparse dictionary and successfully decrease the basis dimensionality and the computational complexity. In a small neighbourhood range, we consider the follow cost function, taking the neighbourhood information and the noise on the reconstruction result into account, to obtain an estimation of the intra-voxel fiber architecture:

$$\begin{aligned} \min \|s - Hw\|_2^2 + \lambda \left(\alpha \|WZ - w\|_2 + \right. \\ \left. (1-\alpha) \|w\|_{\mathrm{TV}}\right) \quad s.t.\ w \geq 0 \end{aligned} \tag{5}$$

where the s represents the measure data, measure matrix H is a result of convolution between the kernel and sparse dictionary derived from section 2.3, which can be depicted as: $H = r(g, v) * f(c, \Omega_c, \xi)$. The second item in above model is the penalty term, whose first part penalizes the difference between the adjacent dictionary coefficients along the underlying fiber orientations and the noise and the latter part is a total variation regularization to the coefficients. The regularization can guarantee the consistency of the fiber orientation to some extent. Parameter λ and α commonly make a trade-off between angular resolution and robustness.

In particularly, matrix $W = [w_1, w_2, \cdots, w_T]$ consists of neighbouring voxels' fODF coefficients, which can be acquired by initialization. Matrix $Z = [\beta_1, \beta_2, \cdots \beta_T]^T$ represents a combination of similarities between center voxel and its neighbours. We measure local structure by calculating the similarity between each voxel and their adjacent elements. The similarity between two voxels is driven by the measure signals via the cosine distance: $\beta_i = 1 - \frac{|s_{\mathcal{F}} \cdot s_i|}{\|s_{\mathcal{F}}\| \|s_i\|}$, which shows the richness of HARDI data information. In intra-voxel field, fibers are natural to be as smooth as possible, while the noise in the data may heavily influence the result of construction. For the purpose of minimizing the undesirable effects caused by noise, we propose to integrate the L1 norm of the image gradient, known as the total variation (TV) [17] regularization, into the penalty term. The TV technique, which is primarily used for image denoising, was shown to have an outstanding ability to smooth away noise in flat regions whilst preserving edges.The above optimization problem can be rewritten to another form as:

$$\begin{aligned} \min \| \left(2H^{\mathrm{T}}H + \lambda\alpha I^{\mathrm{T}} I\right) w - \left(2H^{\mathrm{T}} s + \right. \\ \left. \lambda\alpha WZ\right) \|_2^2 + \lambda (1-\alpha) \|w\|_{\mathrm{TV}} \end{aligned} \tag{6}$$

Note that this is a total variation constrained least-squares problem, which can be conveniently solved by 'DeconvTV' toolbox [18].

Algorithm 1: fODF estimation with ap local feature extraction process

Input: Diffusion signal $s \in \mathbb{R}^n$; Unit hemisphere uniformly sampling vector $\boldsymbol{u} \in \mathbb{R}^m$; Sampling directions $\boldsymbol{v} \in \mathbb{R}^m$ with the tth tessellation of the icosahedron

Output: fODF

Individually calculate the initial fODF set $\tilde{F}$ of ROI according to section 2.1 and 2.2;

while $each\ voxel \in ROI$ **do**

  To the center of the voxel as the T neighborhood, calculate the local regularized problem Eq.(3);

  Search all fODFs to rebuild a new dictionary $\left\{\wp^c_{v^i_j} | v^i_j,\ j = 1, ..., n_i,\ i = 1, ..., \mathrm{T}\right\}$;

  Minimize cost function to compute the coefficient w via Eq.(6);

  Calculate the fODF according to Eq.(4).

end

3 RESULTS

Simulations have been carried out to both study the representational ability of our method which can reconstruct the fiber accurately and verify if and how the proposed algorithm is able to obtain more preferable results with these configurations than Q-ball Imaging and SFM. In the contrast experiments, we utilized the DIPY, which is used in the most popular experiments involving phantom and real data, to obtain the imaging results of Q-ball and SFM.

3.1 Phantom data

To assess the performance of the proposed and reference methods under controllable conditions, one phantom data set produced for the International Symposium on Biomedical Imaging (ISBI) Reconstruction Challenge was used. The data set was acquired from 32 directions with b = 1,200s/mm2 (referred to below as Phantom 1), 64 directions with b = 3,000s/mm2 (referred to below as Phantom 2) with SNR = 10, 20, 30 respectively. A detailed description of the phantom data set can be obtained in ISBI 2013.

As it was mentioned earlier, we compared the performance of three different methods in our simulation study, i.e., q-ball imaging (Q-ball), Sparse Fascicle Model (SFM) and our self-adaptive local feature extracting based imaging method (SLFE). The region of interest (ROI) in the data set has a spatial dimension of 11×11 voxels, and consists of three primary fiber bundles crossing each other. The top row of subplots of Figure 1 show the ground truth of how the fibers distribute. At the same time, the second to fifth rows of subplots of Figure 1 show the fibers recovered by (from left to right) Q-ball, SFM, SLFE. And the fODFs of rows (a, b, c, d) were reconstructed with DTI phantoms, SNR = 10, 30dB and HARDI phantoms, SNR = 10, 30dB respectively. One can see that the Q-ball and SFM failed to clearly represent fibers with a high angle resolution and tended to produce false positive orientations, leading to a poor performance. In addition, the results will be heavily affected when noise degree increases, as the reconstructions were performed on a voxel-by-voxel level with poor noise immunity. On the other hand, the SLFE method, taking the spatial continuity of fibers into account, provided an estimation result of much higher quality. Even the noise level increases, the SLFE can still perform a quite stable and accurate result by incorporating fODFs derived from neighbouring information and TV regularization into the model.

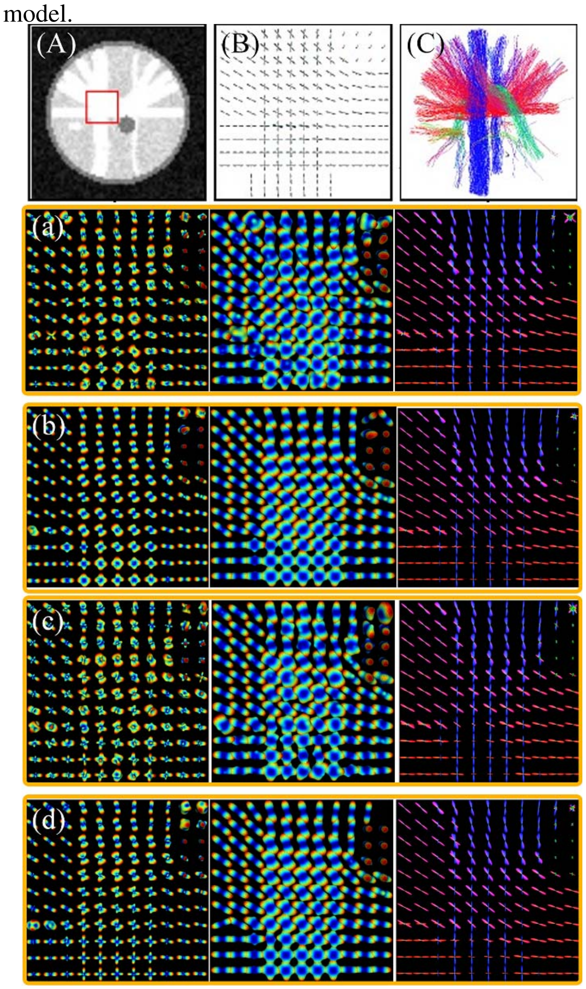

Figure 1: Results of fODFs reconstructed from the ISBI phantom data-set. Upper row of subplots corresponds to the ground truth of fibre distributions. The fODFs were performed by (from left to right) Q-ball, SFM and SLFE. Rows (a) (b) (c) (d): phantom 1 with SNR = 10 and SNR = 30, phantom 2 with SNR = 10 and SNR = 30.

The average angular error(AAE) metric, indicating the deviation of the estimated fiber orientation with the ground truth, was used to quantify the three methods. A detailed analysis about the metric is presented in Figure 2. The plots demonstrate that SLFE outperforms Q-ball and SFM for both phantoms, in three noise conditions. With high quality data (SNR = 30), the differences between the three methods are mild. But the superiority of SLFE compared to Q-ball and SFM appears clearer when we move to severe noise level (SNR=10 and SNR=20). While the average angular error of others ascend dramatically, the AAE of SLFE keeps about 7, showing that the SLFE algorithm is quite robust to noise.

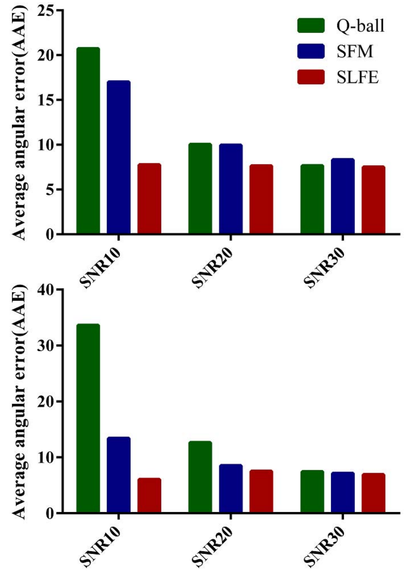

Figure 2: Average angular error(AAE) obtained using the compared methods for phantom 1 (upper) and phantom 2 (bottom), with different SNRs.

3.2 Real data

Experiments with real hardi data were performed in this subsection. The proposed algorithm was tested on human brain scans acquired from a Siemens 3T TIM using SE EPI sequence, with b =2000 s/mm2, 120 gradient directions, and TR/TE = 12400/116 ms. In this data we compared the SLFE method with SFM and Q-ball methods, verified and extended findings from simulation to real data for practical application.

Figure 3 (A-D) shows the intravoxel fiber architecture image of a cross-section of the brain estimated by using the SFM, Q-ball and SLFE methods in a small ROI extracted from the whole brain's fiber imaging. The image displayed on the figure 3(D) is a DWI image of the brain slice in 38th layer, and the area we used to test is labelled with a yellow rectangle. The row groups of subplots show the fODFs estimated by (from up to down) Q-ball, SFM and SLFE. In the fiber region(marked with a yellow box in Figure 3-a), the SFM and SLFE methods are superior to the Q-ball method, which can obtain a smooth fiber architecture with less spurious peaks. As it was already noted earlier, the Q-ball algorithm is sensitive to the noise, tends to result in the disorder of fODF field. The region (marked in Figure 3-b) is a cross-section with a curved fiber bundle and a straight one. As is shown in Figure 3-b, the SLFE algorithm shows a better reconstruction performance, especially in terms of the moothness of fibers, since it takes the continuity of fibers' spatial structure into account. The above conclusion is further supported by an additionpal example(marked with a yellow box in Figure 3-c), which shows the reconstructions pertaining to the indicated area within another section of the brain. Therein, the SLFE can clearly reconstruct different fiber orientations and outperforms the Q-ball and SFM methods.

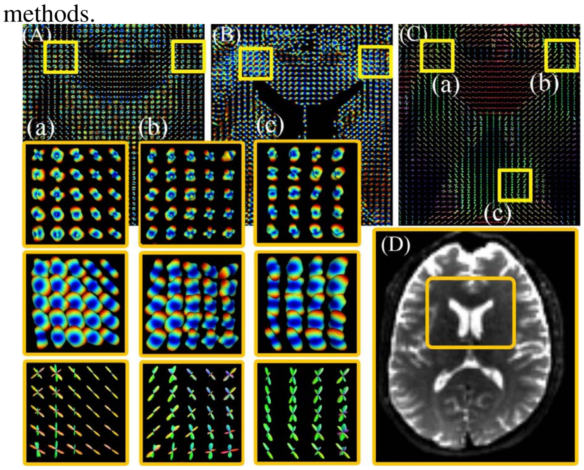

Figure 3: Visualization of the fODFs estimated in a central sagittal brain slice of real single-shell dMRI data. Depicted fODF profiles correspond to the estimates from the Q-ball (A), SFM (B) and SLFE (C) methods.

4 CONCLUSIONS

In this work, we have proposed a data-driven algorithm to recover the intra-voxel fODF from the diffusion data. The method leverages a spatial structured continuity prior on the fODF, where the structure originates from the spatial coherence of the fibre orientation between neighbour voxels. We utilize a sparse dictionary basis to reconstruct the fODF, and the dictionary basis could be constructed in a self-adaptive way, where the basis atoms are extracted from neighbouring voxels' local features, such as original fiber orientations. A total variation regularization is also used to reduce spurious fiber orientation and further decrease the influence of undesirable factors. We have compared the performance of our proposed method with that of Q-ball and SFM methods through numerical simulations and tests on real human data. As shown in section 3, the SLFE algorithm produces a more accurate estimation of fiber orientation and exhibits strong robustness to noise, while the Q-ball imaging method tends to generate some spurious peaks and the SFM shows a deficiency of angular resolution. The SLFE also shows a good ability to recover the fibers with a property of smoothness and spatial continuity. We believe, the presented work has a potential for better assessing white matter structure and connectivity in healthy subjects. A detailed investigation will be shown in the future work.

References

[1] D. K. Jones, T. R. Knsche, and R. Turner, "White matter integrity, fiber count, and other fallacies: The do's and don'ts of diffusion mri," *Neuroimage*, vol. 73, p. 239254, 2013.

[2] T. J-Donald, C. Fernando, and C. Alan, "Robust determination of the fibre orientation distribution in diffusion mri: Non-negativity constrained super-resolved spherical deconvolution," *Neuroimage*, vol. 35, no. 4, p. 14591472, 2007.

[3] D. Christiaens, M. Reisert, T. Dhollander, S. Sunaert, P. Suetens, and F. Maes, "Global tractography of multi-shell diffusion-weighted imaging data using a multi-tissue model," *Neuroimage*, vol. in press, p. 89101, 2015.

[4] D. S. Tuch, "Q-ball imaging.," *Magnetic Resonance in Medicine Official Journal of the Society of Magnetic Resonance in Medicine*, vol. 52, no. 6, pp. 1358–1372, 2004.

[5] J.-D. Tournier, F. Calamante, D. G. Gadian, and A. Connelly, "Direct estimation of the fiber orientation density function from diffusion-weighted mri data using spherical deconvolution," *NeuroImage*, vol. 23, no. 3, pp. 1176–1185, 2004.

[6] M. Reisert, I. Mader, C. Anastasopoulos, M. Weigel, S. Schnell, and V. Kiselev, "Global fiber reconstruction becomes practical," *Neuroimage*, vol. 54, no. 2, pp. 955–962, 2011.

[7] E. J. Canales-Rodríguez, A. Daducci, S. N. Sotiropoulos, E. Caruyer, S. Aja-Fernández, J. Radua, Y. Y. Mendizabal, Y. Iturria-Medina, L. Melie-García, Y. Alemán-Gómez, *et al.*, "Spherical deconvolution of multichannel diffusion mri data with non-gaussian noise models and total variation spatial regularization," *arXiv preprint arXiv:1410.6353*, 2014.

[8] F. Dell'Acqua, P. Scifo, G. Rizzo, M. Catani, A. Simmons, G. Scotti, and F. Fazio, "A modified damped richardson–lucy algorithm to reduce isotropic background effects in spherical deconvolution," *Neuroimage*, vol. 49, no. 2, pp. 1446–1458, 2010.

[9] M. Taquet, B. Scherrer, O. Commowick, J. M. Peters, M. Sahin, B. Macq, and S. K. Warfield, "A mathematical framework for the registration and analysis of multi-fascicle models for population studies of the brain microstructure.," *IEEE Transactions on Medical Imaging*, vol. 33, no. 2, pp. 504–517, 2014.

[10] B. Jeurissen, A. Leemans, J. Tournier, D. Jones, and J. Sijbers, "Estimating the number of fiber orientations in diffusion mri voxels: a constrained spherical deconvolution study," *Proceedings of the International Society for Magnetic Resonance in Medicine. Stockholm, Sweden*, p. 573, 2010.

[11] F. Pestilli, J. D. Yeatman, A. Rokem, K. N. Kay, and B. A. Wandell, "Evaluation and statistical inference for human connectomes," *Nature methods*, vol. 11, no. 10, pp. 1058–1063, 2014.

[12] H. Zou and T. Hastie, "Regularization and variable selection via the elastic net," *Journal of the Royal Statistical Society: Series B (Statistical Methodology)*, vol. 67, no. 2, pp. 301–320, 2005.

[13] J. Mairal, F. Bach, J. Ponce, G. Sapiro, and A. Zisserman, "Non-local sparse models for image restoration," in *Computer Vision, 2009 IEEE 12th International Conference on*, pp. 2272–2279, IEEE, 2009.

[14] M. Rowe, *New tractography methods based on parametric models of white matter fibre dispersion*. PhD thesis, UCL (University College London), 2015.

[15] J. A. Tropp, A. C. Gilbert, and M. J. Strauss, "Algorithms for simultaneous sparse approximation. part i: Greedy pursuit," *Signal Processing*, vol. 86, no. 3, pp. 572–588, 2006.

[16] Y. Wu, Y. Feng, F. Li, and C. F. Westin, "Global consistency spatial model for fiber orientation distribution estimation," in *Biomedical Imaging (ISBI), 2015 IEEE 12th International Symposium on*, 2015.

[17] V. Michel, A. Gramfort, G. Varoquaux, E. Eger, and B. Thirion, "Total variation regularization for fmri-based prediction of behavior," *Medical Imaging, IEEE Transactions on*, vol. 30, no. 7, pp. 1328–1340, 2011.

[18] S. H. Chan, P. E. Gill, and T. Q. Nguyen, "User guide for deconvtv (matlab version 1.0)," 2013.